Threedimensional analytical model for the photodissociation of symmetric triatomics. Absorption and fluorescence spectra of ozone

O. Atabek, M. T. Bourgeois, and M. Jacon

Citation: The Journal of Chemical Physics **84**, 6699 (1986); doi: 10.1063/1.450724
View online: http://dx.doi.org/10.1063/1.450724
View Table of Contents: http://scitation.aip.org/content/aip/journal/jcp/84/12?ver=pdfcov
Published by the AIP Publishing

Three-dimensional analytical model for the photodissociation of symmetric triatomics. Absorption and fluorescence spectra of ozone[a)]

O. Atabek
Laboratoire de Photophysique Moléculaire du CNRS, Université de Paris-Sud, 91405 Orsay, France

M. T. Bourgeois and M. Jacon
Laboratoire de Recherches Optiques et UA 776, Faculté des Sciences, 51062-Reims Cedex, France

(Received 18 December 1985; accepted 7 March 1986)

A full three-dimensional analytical Franck–Condon analysis is presented for dissociative spectroscopies of a symmetric triatomic system. Formulas derived for harmonic potential surfaces are applied to the theoretical calculation of ozone absorption spectrum in the Hartley continuum as well as to the determination of its fluorescence (or resonance Raman) spectrum when submitted to 266 nm wavelength excitation. The Hartley absorption line shape describing the $1\,^1B_2 \leftarrow X\,^1A_1$ photodissociation is reproduced within very good agreement with experiment. The role of the so-called Duschinsky effect originating from the coupling of bending and stretching motions in the excited state is analyzed and comparisons are presented with previous more simple models neglecting this coupling. The influence of temperature is also taken into account through calculations dealing with vibrationally excited species. As for the photoemission fluorescence spectrum carrying a rich information content, the behavior is successfully predicted in its main lines, relative intensities of overtone progressions and of combination bands are fairly well reproduced.

I. INTRODUCTION

Various atmospheric properties, among which the absorbance of solar UV radiation is of recent interest, are modeled using the Hartley ultraviolet absorption continuum of ozone as well as its fluorescence or resonantly enhanced Raman scattering. Many authors have measured the absorption and fluorescence spectra to high precision, at room temperature, and over the range 180–900 K to varying degrees of accuracy.[1–10] The visible-UV spectrum of ozone consists of several band systems: Chappuis (610–550 nm), Huggins (374–310 nm), and Hartley (310–220 nm); all of them being genuinely diffuse, owing to photodissociation into O_2 and O atoms. In the Hartley band, absorption is accompanied by photodissociation within only a few femtoseconds which is a mechanism many orders of magnitude faster than spontaneous emission. This extremely short lifetime of O_3 excited states makes their study by conventional spectroscopic techniques rather difficult. The electronically excited states correspond to unbound potentials upon which dissociation takes place rapidly with near unity quantum yield. Nevertheless a small fraction of absorbed photons is reemitted while the two photofragments are still near each other giving rise to a well-resolved fluorescence spectrum and carrying a rich information content on the high vibrational levels of the $X\,^1A_1$ state as well as on the geometry of the upper state potential $1\,^1B_2$ near its saddle point.[10] Together with numerous studies devoted to the electronic potential energy surfaces of ozone,[11–15] several theoretical models deal with the dynamics of the absorption process such as the frozen Gaussian semiclassical spectral model of Heller,[16] or the Franck–Condon analysis of Adler-Golden.[17] Very good agreement with the experimental absorption spectrum is found at room temperature. The effect of vibrational and rotational excitations built in a temperature-dependent spectrum can also be quantitatively estimated.

We have very recently proposed a full three-dimensional quantum calculation for the accurate evaluation of the vibrational–rotational energy levels in the ground electronic state.[18] The method which is referred to as an optimized basis set close-coupled equations is mainly derived from scattering theory[19–21] and can in principle be applied not only to molecular bound states but also to molecular resonances.[22] However for a symmetric molecule like O_3 the two fragmentation channels $O_2 + O$ or $O + O_2$ are energetically degenerate and this circumstance is a complicating one when this model is considered. A much simpler theory is a Franck–Condon analysis which was initially proposed by Pack[23] in a two-dimensional case and extended by Adler-Golden[17] to three dimensions. The aim of the present paper is to present a full three-dimensional Franck–Condon model which can be worked out in a complete analytical form and applied to the calculation of the absorption and fluorescence spectra. The analytic nature of the model is based upon a quadratic expansion of the ground $X\,^1A_1$ and excited $1\,^1B_2$ potential surfaces in the vicinity of their respective extremum geometry (the minimum in the ground state and the saddle point in the excited state). The bound surface is a harmonic well and the upper surface a harmonic barrier along this coordinate which describes the antisymmetric stretch normal mode in the ground state and the reaction path starting from the barrier top in the excited state. The mixing of the other two coordinates in the excited state known as the Duschinsky effect, is completely taken into account differing in this from Adler-Golden's model for absorption.

Section II calculates the incoming solution of the nonbinding mode of the final state in terms of a hypergeometric function as well as its overlapping with the corresponding binding wave function of the initial state. The calculation of

[a)] Work supported in part by UER 52, Universite Pierre et Marie Curie.

 0021-9606/86/126699-13$02.10

the nonseparable overlap integral resulting from the harmonic wave functions for the other two modes is also indicated. Complete analytical expressions for the absorption cross section and resonance Raman transition probability are given in Sec. III. Section IV is devoted to the detailed discussion of the results. The comparison to Adler-Golden's treatment through a calculation where the Duschinsky effect is neglected constitutes a successful test case. The results are compared to those of other theoretical and experimental treatments for the absorption line shape and to experimental data for the fluorescence spectrum. The role of the Duschinsky effect and the influence of the temperature on the spectrum are analyzed. It is also to be noted that this compact formulation gives a simple and visualizable insight to the dissociative spectroscopy of symmetric triatomic systems.

II. THE MODEL

The electronic absorption spectrum as well as the fluorescence (or resonance Raman) spectrum are monitored by the matrix elements of the dipole moment operator $\mu = \langle \chi_{v_f} \Psi_f | \mu | \Psi_i \chi_{v_i} \rangle$, where Ψ and χ are, respectively, the electronic and nuclear wave functions for the initial (i) and final (f) states, v_i and v_f being convenient collections of internal quantum numbers. An assumption which is referred to as the Condon approximation is to take the electronic dipole matrix element:

$$\mu_{fi} = \langle \Psi_f | \mu | \Psi_i \rangle \tag{1}$$

to be independent of nuclear displacements, at least in a region covered by the spatial extension of χ_{v_i}. This yields the well-known Franck–Condon amplitudes

$$\langle \chi_{v_f} \Psi_f | \mu | \Psi_i \chi_{v_i} \rangle \sim \mu_{fi} \langle \chi_{v_f} | \chi_{v_i} \rangle . \tag{2}$$

One of the simplest ways to obtain these overlaps is to restrict their calculation to regions, where low v_i of the ground state being considered, the χ_{v_i} are localized and use quadratic approximations to the local potential surfaces.

The ground electronic state $X\,^1A_1$ of O_3 is binding in all directions and is described in terms of its normal vibration coordinates q_1,q_2,q_3 (symmetric stretch, bend, asymmetric stretch, respectively):

$$V_{X\,^1A_1}(q_1,q_2,q_3) = \tfrac{1}{2}k_{11}q_1^2 + \tfrac{1}{2}k_{22}q_2^2 + \tfrac{1}{2}k_{33}q_3^2 . \tag{3}$$

The excited electronic state $1\,^1B_2$ is still binding with respect to the dissociation into atoms (O + O + O), but unbound and repulsive for dissociation to an O_2 molecule and an O atom. The bending angle being kept fixed, this surface has the appearance of two symmetric valleys each describing the half-reactions O + O_2 or O_2 + O with a saddle point lying along the bisector of the axes for O–O distances. The appropriate coordinates to use on it are the reaction coordinates q_1',q_2',q_3'.[24–26] More precisely q_3' measures the distance along the reaction path from the barrier top, q_1' and q_2' the vibrational motions orthogonal to q_3'. Asymptotically q_1' and q_2' describe the O_2 fragment vibration coordinate and its rotation as referenced to the vector joining the O atom to the center of mass of O_2, the length of which is q_3'. Near the top of the barrier, as a consequence of symmetry the reaction coordinate q_3' is parallel to the corresponding normal mode q_3 of the ground state. On the contrary, (q_1',q_2') can be related to (q_1,q_2) by a rotation known as the Duschinsky effect. Finally, the potential surface for the $1\,^1B_2$ state has the following quadratic form when expressed in terms of the $X\,^1A_1$ state normal coordinates:

$$V_{1\,^1B_2}(q_1,q_2,q_3) = \tfrac{1}{2}k'_{11}(q_1-\bar{q}_1)^2 + \tfrac{1}{2}k'_{22}(q_2-\bar{q}_2)^2 - \tfrac{1}{2}k'_{33}q_3^2 + k'_{12}q_1q_2 + \Delta, \tag{4}$$

where $\bar{q}_1,\bar{q}_2$ indicate the location of the saddle point with respect to the minimum of $V_{X\,^1A_1}$ along the bisector, Δ is an electronic positioning constant. In the upper state, symmetry dictates that linear terms in q_3 vanish and the saddle point and the minimum must lie along the bisector, $\bar{q}_3 = 0$. All positioning and force constants are estimated from available data, resulting from *ab initio* calculations[13,27,28] and analysis of absorption and resonance Raman spectra.[10] They are given in Table I.

As q_3 is completely decoupled from q_1 and q_2, the Franck–Condon amplitudes we are looking for can be separated into two integrals:

$$\langle \chi_{v_f} | \chi_{v_i} \rangle = W_{v_3}(f,E_f) \cdot W_{v_1v_2}(v_1',v_2') \tag{5}$$

namely one $W_{v_3}(f,E_f)$ which is one-dimensional and the other $W_{v_1v_2}(v_1',v_2')$ two-dimensional, the condensed notations meaning

$$W_{v_3}(f,E_f) = \langle \chi^-_{f,E_f}(q_3) | \chi_{v_3}(q_3) \rangle_{q_3} \tag{6}$$

and

$$W_{v_1v_2}(v_1',v_2') = \langle \chi_{v_1'}(q_1')\chi_{v_2'}(q_2') | \chi_{v_1}(q_1)\chi_{v_2}(q_2) \rangle_{q_1,q_2} . \tag{7}$$

$\chi_{v_1}(q_1), \chi_{v_2}(q_2), \chi_{v_3}(q_3)$ are the harmonic oscillator wave functions describing the three normal modes of the initial $X\,^1A_1$ state. $\chi_{v_1'}(q_1'), \chi_{v_2'}(q_2')$ designate the corresponding modes for the binding degrees of freedom of the final $1\,^1B_2$ state. $\chi^-_{f,E_f}(q_3)$ is the "incoming" solution of the remaining nonbinding mode of the final state that evolves in the distant future to a well-defined state of the fragments, f being the fragment channel index.[29] In order to build such an eigen-

TABLE I. Parameters used in the calculations.

Matrix transformation between normal modes and reaction coordinates

$$\begin{pmatrix} q_1' \\ q_2' \end{pmatrix} = \begin{pmatrix} \cos\theta & \sin\theta \\ -\sin\theta & \cos\theta \end{pmatrix} \begin{pmatrix} q_1 \\ q_2 \end{pmatrix} - \begin{pmatrix} 0.552 \\ 0.512 \end{pmatrix}$$

$\theta = 0.1143$ rad

Force constants ($\times 10^{29}$ s^{-2})

Ground state[a]	Excited state[b]
$k_{11} = 0.4576$	$k'_{11} = 0.2628$
$k_{22} = 0.1821$	$k'_{22} = 0.4630$
$k_{33} = 0.4215$	$k'_{33} = -0.4797$

Normal mode frequencies (cm^{-1})

$\omega_1 = 1134.9$	$\omega_1' = 860.0$
$\omega_2 = 716.0$	$\omega_2' = 361.0$
$\omega_3 = 1089.2$	$\omega_3' = 1162.0$

[a] Taken from Ref. 28.
[b] Taken from Ref. 27.

vector we have to look for the continuum wave function of the parabolic barrier problem

$$\left(-\frac{\hbar^2}{2}\frac{d^2}{dq_3^2}-\frac{1}{2}k'_{33}q_3^2-E_f\right)\chi_{E_f}^{\eta}(q_3)=0. \tag{8}$$

The analytic solutions of Eq. (8) have already been derived in the literature.[30,31] One finds the two following linearly independant eigenvectors of even and odd parity according to the value of η (0 or 1/2, respectively):

$$\chi_{E_f}^{\eta}(q_3)=N^{\eta}(\epsilon)\xi^{2\eta}\exp\left(-\frac{i}{2}\xi^2\right)\times{}_1F_1\left(\frac{1}{4}+\eta+i\frac{\epsilon}{2};\frac{1}{2}+2\eta;i\xi^2\right) \tag{9}$$

expressed in terms of dimensionless variables

$$\xi=(k'_{33}/\hbar^2)^{1/4}q_3$$

and

$$\epsilon=(\hbar^2k'_{33})^{-1/2}E_f, \tag{10}$$

where ${}_1F_1(a;c;z)$ is a degenerate hypergeometric function.[32] The appropriate energy-normalization factor $N^{\eta}(\epsilon)$ leading to

$$\langle\chi_{E_f}^{\eta}(q_3)|\chi_{E'_f}^{\eta'}(q_3)\rangle_{q_3}=\delta(E_f-E'_f)\delta_{\eta\eta'} \tag{11}$$

is derived in Appendix A and results in

$$N^{\eta}(\epsilon)=(2\pi)^{-1}\hbar^{-3/4}k'^{-1/8}_{33}(1-\eta)^{-1}\times\exp(\pi\epsilon/4)\left|\Gamma\left(\frac{1}{4}+\eta+i\frac{\epsilon}{2}\right)\right|. \tag{12}$$

The asymptotic behavior of these wave functions can easily be derived from the limiting expressions of the hypergeometric function.[32] The results are

$$\lim_{q_3\to\pm\infty}\chi_{E_f}^{\eta}(q_3)=(\pm1)^{2\eta}N^{\eta}(\epsilon)\lambda^{-1/2}A(\epsilon,\eta)|q_3|^{-1/2}\times\exp(-i\lambda^2q_3^2/2)\exp[-i\epsilon\ln(\lambda|q_3|)]+\text{c.c.}, \tag{13}$$

where

$$A(\epsilon,\eta)=(1/2)^{2\eta}\pi^{1/2}\exp\left(-\frac{\pi\epsilon}{4}+i\frac{\pi}{8}+i\eta\frac{\pi}{2}\right)\times\left[\Gamma\left(\frac{1}{4}+\eta-i\frac{\epsilon}{2}\right)\right]^{-1}; \tag{14}$$

c.c. means the complex conjugate expression and $\lambda=(k'_{33}/\hbar^2)^{1/4}$.

The definition of the incoming wave $\chi_{fE_f}^{-}$ which is a linear combination of the two independent even and odd parity solutions of Eq. (8):

$$\chi_{fE_f}^{-}(q_3)=a_f(E_f)\chi_{E_f}^{\eta=1/2}(q_3)+b_f(E_f)\chi_{E_f}^{\eta=0}(q_3) \tag{15}$$

proceeds through the specification of the asymptotic behavior in the dissociation valleys. Namely the values 1 or 2, f takes, will correspond to an absence of outgoing wave in $q_3\to-\infty$ or $q_3\to+\infty$ directions, respectively. These two solutions are obtained by setting the amplitude of the outgoing wave {i.e., $\exp[i\epsilon\ln(\lambda|q_3|)]$} to a null value either for $q_3\to-\infty$ ($f=1$) or for $q_3\to+\infty$ ($f=2$). The resulting two equations

$$a_f(E_f)A^*(E_f,1/2)+(-1)^fb_f(E_f)A^*(E_f,0)=0;\quad(f=1,2) \tag{16}$$

give the ratio of the energy-dependent a and b coefficients. The complete derivation of $\chi_{fE_f}^{-}(q_3)$ is achieved by energy normalization:

$$\chi_{fE_f}^{-}(q_3)=\frac{1}{\sqrt{2}}\left[\frac{\Gamma[3/4+i(\epsilon/2)]}{|\Gamma[3/4+i(\epsilon/2)]|}\chi_{E_f}^{\eta=1/2}(q_3)+(-1)^{f+1}\times\exp(-i\pi/4)\frac{\Gamma[1/4+i(\epsilon/2)]}{|\Gamma[1/4+i(\epsilon/2)]|}\chi_{E_f}^{\eta=0}(q_3)\right];\quad(f=1,2). \tag{17}$$

The different ingredients comprising the Franck–Condon amplitude [Eq. (5)] are thus analytically derived.

Furthermore the integrals themselves are also analytical. The evaluation of the two-dimensional overlaps $W_{v_1v_2}(v'_1,v'_2)$ between harmonic oscillator wave functions for the q_1 and q_2 modes is a well known procedure.[35,36] Due to the mixing of the normal mode coordinates in the final electronic state, the determination of $W_{v_1v_2}(v'_1,v'_2)$ amounts to the calculation of two-dimensional nonseparable Franck–Condon amplitudes. This coordinate mixing induced by a nonnegligible k'_{12} in Eq. (4) influences the spectrum in a manner known as the Duschinsky effect. Coordinates (q'_1,q'_2) are related to (q_1,q_2) by a matrix transformation which is completely determined by the force constants and the equilibrium geometry in both electronic states[37]:

$$\mathbf{q}'=\mathbf{Tq}+\mathbf{D}. \tag{18}$$

Explicit forms for matrices **T** and **D** are indicated in Table I and the calculation of $W_{v_1v_2}(v'_1,v'_2)$ is described in Appendix B. The method consists in expressing these integrals as linear combinations of products of one-dimensional integrals which in turn are evaluated using a recursive procedure described by Manneback.[38] As for the one-dimensional overlap integral of the q_3 mode $W_{v_3}(f,E_f)$ a full analytical expression is worked out in the next section.

III. ABSORPTION AND RESONANCE RAMAN INTENSITIES

The first order absorption or dissociation cross section is given by the usual Golden Rule formula

$$\sigma_{v_1v_2v_3}(\hbar\omega)\sim\mu_{fi}^2\sum_{v'_1v'_2f}|W_{v_1v_2}(v'_1,v'_2)\cdot W_{v_3}(f,E_f)|^2. \tag{19}$$

The sum is over all final states that are accessible with a photon of frequency ω. E_f is the energy available for the unbounded motion in the q_3 direction and its value is governed by energy conservation law

$$E_f=\hbar\omega+\hbar\omega_1(v_1+1/2)+\hbar\omega_2(v_2+1/2)+\hbar\omega_3(v_3+1/2)-\hbar\omega'_1(v'_1+1/2)-\hbar\omega'_2(v'_2+1/2)-\Delta. \tag{20}$$

According to an argument presented by Pack,[23] because the minima of the $1\,^1B_2$ potential in q_1 and q_2 directions are shifted from those of the $X\,^1A_1$ state, the two-dimensional overlaps $W_{v_1v_2}(v_1',v_2')$ will have appreciable values for a number of excited v_1',v_2' levels and will be responsible for the large overall Franck–Condon envelope. As for $W_{v_3}(f,E_f)$, if ω is such that the available energy E_f is much below the top of the barrier, there is a negligible amplitude of the continuum wave function in the region where $\chi_{v_3}(q_3)$ is large, resulting in a negligible overlap. The same conclusion is valid if E_f is much above the barrier as rapid oscillations of the continuum wave function cancel the overlap. A large overlap can only be achieved when E_f is very near the top of the barrier so that $W_{v_3}(f,E_f)$ is responsible for some sharp individual peaks, one for each vibrational state (v_1',v_2'), that are superimposed to the large absorption band. This interpretation might well be at the origin of the structures observed on the Hartley continuum of ozone. Unfortunately, as already shown by Adler-Golden,[17] the spacing between these peaks governed by the vibrational level spacing in the q_1' and q_2' motions is too small ($\sim 200\ \mathrm{cm}^{-1}$) when compared to $\omega_1 = 860\ \mathrm{cm}^{-1}$ and $\omega_2 = 361\ \mathrm{cm}^{-1}$.

Let us now consider the resonance Raman process describing the inelastic scattering of a photon of frequency ω hitting the triatomic molecule in its initial ground electronic state $X\,^1A_1$, characterized by its internal quantum numbers v_1,v_2,v_3, and leaving it in the same electronic but $\tilde{v}_1,\tilde{v}_2,\tilde{v}_3$ vibrational state, the transition occurring via the excited electronic state $1\,^1B_2$. At the lowest order in molecule-field coupling, the well known formula for the transition probability is[39]

$$I_{\tilde{v}_1\tilde{v}_2\tilde{v}_3,v_1v_2v_3}(\hbar\omega) \sim \mu_{fi}^4 \left| \lim_{\alpha\to 0^+} \sum_{v_1'v_2'f} \int \frac{W^*_{\tilde{v}_1\tilde{v}_2}(v_1',v_2')\, W^*_{\tilde{v}_3}(f,E_f)\, W_{v_3}(f,E_f)\, W_{v_1v_2}(v_1',v_2')}{\hbar\omega - E_{v_1'v_2'} - E_f + i\alpha}\, dE_f \right|^2, \tag{21}$$

where

$$E_{v_1'v_2'} = \hbar\omega_1'(v_1' + 1/2) + \hbar\omega_2'(v_2' + 1/2). \tag{22}$$

Here again, due to the separation of the variable q_3 from (q_1,q_2), Eq. (21) can be recast in the form

$$I_{\tilde{v}_1\tilde{v}_2\tilde{v}_3;v_1v_2v_2}(\hbar\omega) \sim \mu_{fi}^4 \left| \sum_{v_1'v_2'} W^*_{\tilde{v}_1\tilde{v}_2}(v_1',v_2')\, \mathscr{A}^{v_1'v_2'}_{\tilde{v}_3v_3}(\hbar\omega)\, W_{v_1v_2}(v_1',v_2') \right|^2, \tag{23}$$

where the amplitude $\mathscr{A}$ is

$$\mathscr{A}^{v_1'v_2'}_{\tilde{v}_3v_3}(\hbar\omega) = \lim_{\alpha\to 0^+} \sum_f \int \frac{W^*_{\tilde{v}_3}(f,E_f)\, W_{v_3}(f,E_f)}{\hbar\omega - E_{v_1'v_2'} - E_f + i\alpha}\, dE_f. \tag{24}$$

Further progress concerning both the calculation of the absorption cross section [Eq. (19)] and of the resonance Raman intensity [Eq. (23)] requires the evaluation of the key quantity $W_{v_3}(f,E_f)$. In the case of the parabolic barrier a complete analytical derivation is possible. This is based, together with the expression of the outgoing wave function [Eq. (17)], upon the possibility of expressing the usual Hermite polynomial form of harmonic oscillator wave functions in terms of hypergeometric functions[34]:

$$\chi_{v_3}(q_3) = M(2\beta q_3)^{2\eta} \exp(-\beta^2 q_3^2/2) \times {}_1F_1(-p;\tfrac{1}{2} + 2\eta;\beta^2 q_3^2), \tag{25}$$

where the integers v_3 and p are related by

$$v_3 = 2(p + \eta), \tag{26}$$

η taking, as previously, the values 0 or 1/2 for even or odd parity. The normalization factor M is given by

$$M = (-1)^p (k_{33}/\pi^2\hbar^2)^{1/8} 2^{-v_3/2} (v_3!)^{1/2} (p!)^{-1} \tag{27}$$

and

$$\beta = (k_{33}/\hbar^2)^{1/4}. \tag{28}$$

According to the parity of the initial bound function χ_{v_3} either $\langle \chi^{\eta=1/2}_{E_f} | \chi_{v_3} \rangle$ or $\langle \chi^{\eta=0}_{E_f} | \chi_{v_3} \rangle$ will drop when the overlap between the wave functions given by Eqs. (17) and (25) is calculated. The summation over f being performed the result can be recast in the form

$$\sum_f |W_{v_3}(f,E_f)|^2 = |\langle \chi^{\eta}_{E_f}(q_3) | \chi_{v_3}(q_3) \rangle|^2. \tag{29}$$

A compact form for $\Sigma_f |W_{v_3}(f,E_f)|^2$, convenient for both parities, is then

$$\sum_f |W_{v_3}(f,E_f)|^2 = \left| \frac{1}{2} M N^{\eta}(E_f) (2\lambda\beta)^{2\eta} \int_0^\infty \exp[(-\beta^2 + i\lambda^2)u/2] u^{2\eta - 1/2}\, {}_1F_1\left(-p;\frac{1}{2} + 2\eta;\beta^2 u\right) \times {}_1F_1\left(\frac{1}{4} + \eta + i\frac{\epsilon}{2};\frac{1}{2} + 2\eta;i\lambda^2 u\right) du \right|^2, \tag{30}$$

where the change of variable $u = q_3^2$ is done. The integration implied by Eq. (30) can be analytically performed and results (cf. Ref. 34, pp. 47 and 64) after some algebra in

$$\sum_f |W_{v_3}(f,E_f)|^2 = \left|(-1)^p 2^{3\eta-p-1/2}\pi^{-5/4}(v_3!)^{1/2}(p!)^{-1}(1-\eta)^{-1}\chi^{-1/8+\eta/2}k_{33}^{-1/4}\right.$$
$$\times\exp(\epsilon\gamma/2)\left|\Gamma\left(\frac{1}{4}+\eta+i\frac{\epsilon}{2}\right)\right|\left[\Gamma\left(2\eta+\frac{1}{2}\right)\right]^2\left[\Gamma\left(\frac{1}{4}+\eta+i\frac{\epsilon}{2}\right)\right]^{-1}$$
$$\times\sum_{q=0}^{p}(-2)^q C_p^q(1+\chi)^{-1/2(q+2\eta+1/2)}\exp\left[-\frac{i}{2}q\left(\gamma-\frac{\pi}{2}\right)\right]\Gamma\left(\frac{1}{4}+q+\eta+i\frac{\epsilon}{2}\right)$$
$$\left.\times\left[\Gamma\left(\frac{1}{2}+2\eta+q\right)\right]^{-1}{}_2F_1\left(\frac{1}{4}+\eta-i\frac{\epsilon}{2},-q;\frac{3}{4}-q-\eta-i\frac{\epsilon}{2};\frac{1-i\chi^{1/2}}{1+i\chi^{1/2}}\right)\right|^2 \tag{31}$$

with

$$\chi = k'_{33}/k_{33} \tag{32}$$

and

$$\gamma = \frac{\pi}{2} + \arg(1-\chi-2i\chi^{1/2}). \tag{33}$$

A particular case of this expression for $v_3 = 0$ has been previously obtained by Plotnikov.[30] Equations (19) and (31) give the complete analytic formula for the absorption cross section governed by a sum of generalized hypergeometric functions ${}_2F_1$ of complex argument which can be numerically evaluated using accurate standard algorithms.

As for the cross section of the Raman scattering process, $W_{v_3}(f,E_f)$ is involved in an integral form as is seen from Eq. (24). In the case where v_3 and $\tilde{v}_3$ are of different parities (even for v_3, odd for $\tilde{v}_3$ for example):

$$W^*_{\tilde{v}_3}(f,E_f)W_{v_3}(f,E_f) = (-1)^{f+1}\frac{1}{2}e^{-i(\pi/4)}$$
$$\times\frac{\Gamma^*[\frac{1}{4}+i(\epsilon/2)]\Gamma[\frac{3}{4}+i(\epsilon/2)]}{|\Gamma[\frac{1}{4}+i(\epsilon/2)]|\,|\Gamma[\frac{3}{4}+i(\epsilon/2)]|}$$
$$\times\langle\chi_{\tilde{v}_3}|\chi_{E_f}^{\eta=1/2}\rangle\langle\chi_{E_f}^{\eta=0}|\chi_{v_3}\rangle \tag{34}$$

and the summation over f results in a null contribution:

$$\sum_f W^*_{\tilde{v}_3}(f,E_f)W_{v_3}(f,E_f) = 0. \tag{35}$$

On the contrary when v_3 and $\tilde{v}_3$ are of the same parity (even for example):

$$W^*_{v_3}(f,E_f)W_{v_3}(f,E_f) = (-1)^{2f}\tfrac{1}{2}\langle\chi_{\tilde{v}_3}|\chi_{E_f}^{\eta=0}\rangle\langle\chi_{E_f}^{\eta=0}|\chi_{v_3}\rangle \tag{36}$$

and the summation over f gives

$$\sum_f W^*_{\tilde{v}_3}(f,E_f)W_{v_3}(f,E_f) = \langle\chi_{\tilde{v}_3}|\chi_{E_f}^{\eta=0}\rangle\langle\chi_{E_f}^{\eta=0}|\chi_{v_3}\rangle, \tag{37}$$

where both of the products of the right-hand side can be obtained from Eq. (31). As a partial result of this analysis we can say that we will not observe Raman scattering with $\Delta v_3 = \pm 1$. A nonzero amplitude $\mathscr{A}_{\tilde{v}_3 v_3}$ can be analytically evaluated for any $v_3,\tilde{v}_3$ having the same parity and results in a cumbersome but compact formula (see derivation in Appendix C), but it can also be given a three terms recursive form starting from $\mathscr{A}_{00}$ and $\mathscr{A}_{11}$. This is based on the representation of $\mathscr{A}$ in terms of the resolvent operator[40] of the q_3 mode in the excited state:

$$\mathscr{A}^{v_1'v_2'}_{\tilde{v}_3 v_3}(\hbar\omega) = \langle\chi_{\tilde{v}_3}|(Z-H_f)^{-1}|\chi_{v_3}\rangle, \tag{38}$$

where

$$Z = \hbar\omega - E_{v_1'v_2'} - E_f + i\alpha. \tag{39}$$

The Hamiltonian

$$H_f = p_3^2/2 - \tfrac{1}{2}k'_{33}q_3^2, \tag{40}$$

where p_3 is the momentum associated to q_3, can be written in terms of the creation and annihilation operators of the initial q_3 harmonic oscillator as

$$H_f = -\frac{\hbar^4}{4}k'^{1/2}_{33}$$
$$\times[(1+\chi)(a^2+a^{+2}) - (1-\chi)(aa^+ + a^+a)]. \tag{41}$$

Explicit expressions for a and a^+ are given by

$$a = 2^{-1/2}[(k_{33}/\hbar^2)^{1/4}q_3 + i(\hbar^2 k_{33})^{1/4}p_3], \tag{42a}$$
$$a^+ = a^*. \tag{42b}$$

Here again, from Eq. (41), we observe that only two-photon or zero-photon transitions inducing $\Delta v_3 = 0, \pm 2$ changes are possible. This is clearly shown from the identity

$$\sum_w \langle\chi_{\tilde{v}_3}|(Z-H_f)^{-1}|\chi_w\rangle\langle\chi_w|(Z-H_f)|\chi_{v_3}\rangle = \delta_{\tilde{v}_3 v_3} \tag{43}$$

which leads to

$$\mathscr{A}^{v_1'v_2'}_{\tilde{v}_3 v_3+2}(1+\chi)(v_3+1)^{1/2}(v_3+2)^{1/2}$$
$$+\mathscr{A}^{v_1'v_2'}_{\tilde{v}_3 v_3}\left[\frac{4}{\hbar\omega_3}Z + (1-\chi)(2v_3+1)\right]$$
$$+\mathscr{A}^{v_1'v_2'}_{\tilde{v}_3 v_3-2}(1+\chi)v_3^{1/2}(v_3-1)^{1/2} = -\frac{4}{\hbar\omega_3}\delta_{\tilde{v}_3 v_3}. \tag{44}$$

$\mathscr{A}^{v_1'v_2'}_{00}$ and $\mathscr{A}^{v_1'v_2'}_{11}$ can be obtained from the general formula given in Appendix C:

$$\mathscr{A}^{v_1'v_2'}_{00} = -ik'^{1/2}_{33}\chi^{-1/4}(1+\chi)^{-1/2}\Gamma\left(\frac{1}{4}-i\frac{Z}{2}\right)$$
$$\times\left[\Gamma\left(\frac{5}{4}-\frac{i}{2}Z\right)\right]^{-1}\exp(-i\gamma/2)$$
$$\times{}_2F_1\left(\frac{1}{4}-i\frac{Z}{2};\frac{1}{2};\frac{5}{4}-i\frac{Z}{2};-e^{-2i\gamma}\right) \tag{45}$$

and

$$\mathscr{A}_{11}^{v_1'v_2'} = -ik\,{}_{33}^{1/2}8\pi^{-1/2}\chi^{1/4}(1+\chi)^{-3/2}\exp(-3i\gamma/2) \times\Gamma\left(\frac{3}{4}-i\frac{Z}{2}\right)\Gamma\left(\frac{3}{2}\right)\left[\Gamma\left(\frac{7}{4}-i\frac{Z}{2}\right)\right]^{-1} \times{}_2F_1\left(\frac{3}{4}-i\frac{Z}{2};\frac{3}{2};\frac{7}{4}-i\frac{Z}{2};-e^{-2i\gamma}\right). \tag{46}$$

Finally Eqs. (44)–(46) or Eqs. (23) and (C13) give the complete analytical expression for the resonance Raman intensity either in a recursive or compact form.

IV. RESULTS

The absorption and fluorescence spectra induced by the single q_3 mode deserve interest for themselves as the observed line shapes and Raman transition probabilities [Eqs. (19) and (23)] appear to be sums of bound-free overlaps $W_{v_3}(f,E_f)$ weighted by the Franck–Condon factors of the two other q_1 and q_3 modes.

Figures 1 and 2 display typical plots for the square of bound-free integrals $\Sigma_f|W_0(f,E_f)|^2$ and that of transition amplitudes $|\mathscr{A}_{0v_3}|^2$ given by formulas (31) and (44)–(46) as a function of the energy available for the continuum motion. A relevant parameter, when the symmetry with respect to the energy of the top of the barrier is considered, is χ [Eq. (32)] which measures the ratio of frequencies in the q_3 mode for the upper and lower electronic states. When these frequencies are taken to be equal, ($\chi = 1$), γ given by Eq. (33) is null, the consequence being a symmetric profile for the absorption or the fluorescence. This can easily be seen by inspection of Eqs. (31) and (C16) where the only energy dependent factor which can induce an asymmetry, namely $\exp(\epsilon\gamma/2)$, is unity. For all other cases these profiles show an asymmetric behavior with either a broadening for increasing energies (with $\chi<1$) or for decreasing energies (with $\chi>1$) in the case of the absorption and the reverse for fluorescence.

An interesting feature of the absorption peaks is that, as pointed out by Pack,[23] their widths are controlled by the curvature of the top of the barrier, which is measured by the q_3 normal frequency in the upper state. More precisely the widths are equal to these frequencies, so that the smaller the curvature, the narrower the peaks.

As for the symmetric fluorescence profiles, a nearly energy-independent behavior of $|\mathscr{A}_{02}|^2$ is to be pointed out. This can be analyzed as a consequence of Eq. (44), where for $\chi = 1$ one has

$$|\mathscr{A}_{02}|^2 = \frac{4}{\hbar^2\omega_3'^2}[1+Z\mathscr{A}_{00}]^2. \tag{47}$$

Within the energy range corresponding to the absorption ($\sim\hbar\omega_3'$), $Z\mathscr{A}_{00}$ has a negligible contribution (less than 1%) inducing an approximately constant $|\mathscr{A}_{02}|^2$. From the same Eq. (44), we can recursively show that all $|\mathscr{A}_{0v_3}|^2$, with $v_3 = 4p+2$, have this common behavior.

We are now in a position to analyze the results of our calculations as applied to the interpretation of the Hartley absorption band and the resonance fluorescence spectrum.

A. Hartley absorption band

This absorption line shape has been extensively studied by several authors[5,6,13,27,41,42] and in particular by Adler-Golden[17] with quite good agreement with the observed spectrum. The analytical model we have so far developed in this work is an improvement over that of Ref. 17 in the sense that it takes into account the so-called Duschinsky effect arising from nonseparable bound–bound integrals.

As a test case we take the parameters of Ref. 17 model 2b, where the $1\,{}^1B_2$ potential surface presents a substantially different equilibrium bond angle than in the ground state and also by neglecting the Duschinsky effect, we reproduce Adler-Golden's results within very good agreement. Returning to our model we note that for the force constants

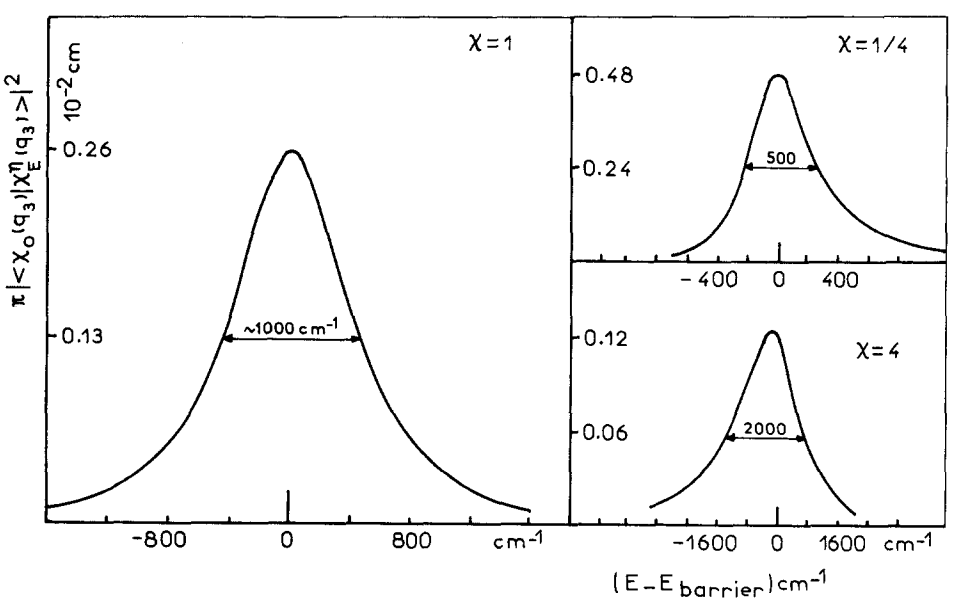

FIG. 1. Bound-free Franck–Condon factors as a function of the energy available for the continuum motion, for different values of the asymmetry parameter χ.

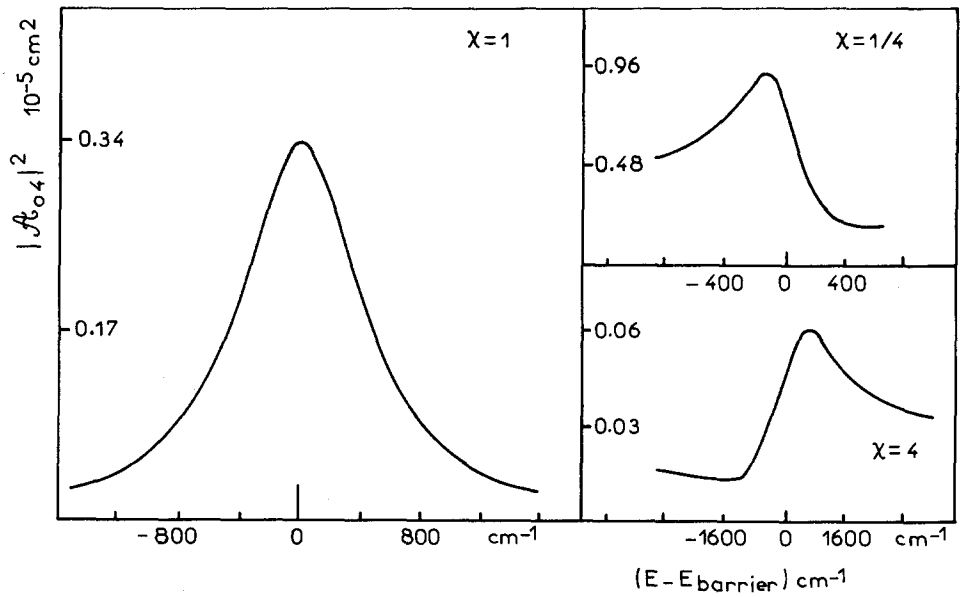

FIG. 2. Typical fluorescence profiles for different values of the asymmetry parameter χ.

listed in Table I, the calculations lead to a rather narrow profile with peaks positioned at energies corresponding to the frequencies of q_1 and q_2 modes in conformity to Pack's assessment.

Although experimentally such structures are present in the Hartley band, the peaks we are calculating cannot correspond to them as their observed spacing is much lower (200–300 cm^{-1}) than the vibrational level spacing in the q_1 or q_2 motion in the upper state ($\omega_1 = 860\,cm^{-1}, \omega_2 = 361\,cm^{-1}$). To get a correct width we have to increase the q_3 normal mode frequency ω_3' in the upper state as is done by Adler-Golden, from 1161 to 1900 cm^{-1} for which a very good fit is obtained when compared to the experimental spectrum at low temperature ($T = 223$ K). We note that with this value for ω_3' the fine structure arising from q_1 and q_2 modes is practically washed out. Figure 3(a) displays together with the experimental results our calculated Hartley continuum absorption line shape from the vibrational ground state (0,0,0). Figure 3(b) collects the corresponding profiles for vibrationally excited states (1,0,0),(0,1,0),(0,0,1) showing a bimodal behavior slightly more asymmetric ($\sim 6\%$) than the one calculated by Adler-Golden.[17] Figure 4 summarizes the role of the Duschinski effect. A calculation incorporating it leads to an absorption profile slightly collapsed (overall intensity decrease of 9%, extrabroadening of 8%) and slightly blue shifted (~ 300 cm^{-1}). Finally, calculations taking into account the temperature dependence of the Hartley band through the Boltzmann weighted combination of absorption line shapes from the vibrationally ground (0,0,0) and excited states (1,0,0), (0,1,0), and (0,0,1) show only very slight modifications between 223 and 293 K. More precisely they correspond to a collapse ($\sim 1\%$) of the 293 K line shape when compared to the 223 K one. These results are in agreement with some recent observations.[42]

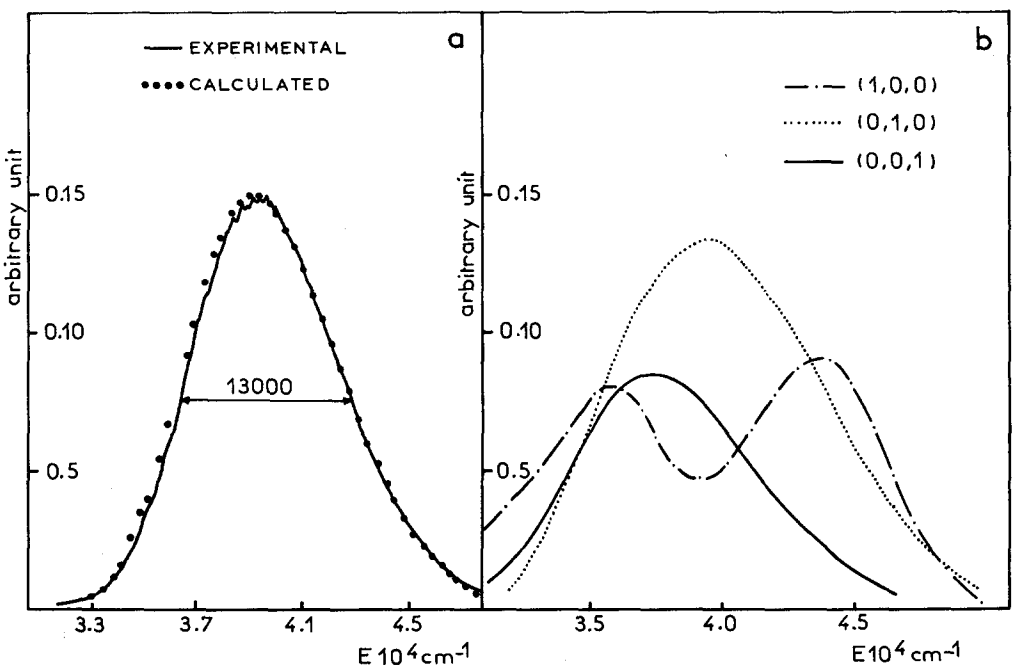

FIG. 3. Hartley continuum absorption from vibrationally ground (a) or excited states (b).

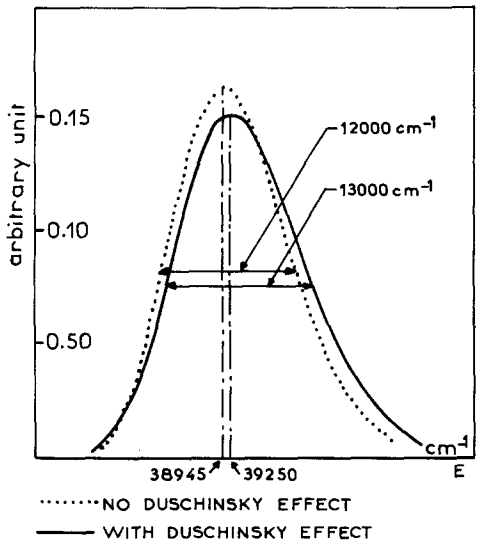

FIG. 4. Role of the Duschinsky effect in Hartley continuum absorption from vibrationally ground state.

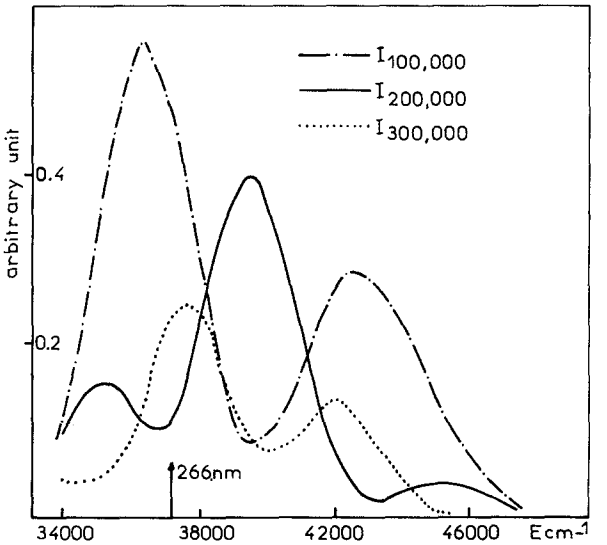

FIG. 5. Raman excitation profiles for the ν_1 progression from the ground (0,0,0) state. The arrow indicates the position of the excitation wavelength used when obtaining the photoemission spectrum (see the text).

B. Fluorescence spectrum

Although the upper electronic state of ozone is highly repulsive leading to rapid dissociation following excitation in the Hartley band with near unity quantum yield, photoemission of sufficient intensity has also been observed. Such inelastically scattered light recorded as a well-resolved fluorescence spectrum is very helpful in determining the geometry of the upper state potential energy surface near its saddle point. The low resolution spectrum of ozone excited at 266 nm wavelength within the maximum of the Hartley band consists of a long progression in ν_1 overtones (in the q_1 symmetric stretch) as well as combination bands in ν_1 and even quanta of ν_3 (in the q_3 antisymmetric stretch).[10] One also observes a progression of ν_3 overtones with even quanta but no bands with $\nu_2 \neq 0$ (excitation of the q_2 bending mode) are evident. The progression of the ν_1 symmetric mode which is a characteristic feature of the resonance Raman spectrum has already been studied[43] but, to our knowledge, the semiclassical work of Heller and co-workers[44] is the only one which is devoted to the interpretation of q_3 mode Raman profiles. The analytical model which is of interest here, although based on a very rough estimation of the upper state surface which can only make sense in the vicinity of the saddle point leads, through the calculation of band intensities, to a reasonably fair reproduction of the main features of the spectrum. When taking into account the extreme sensitiveness of the Raman spectrum on the details of the potential surface, these results are very encouraging.

The relative intensities of the vibrational bands are simply deduced from peak intensities of the spectrum which may induce rather poor estimates in regions of important overlapping. On the other hand a parameter which is not controlled is the temperature of target molecules interacting with the laser. Calculations have thus been limited only to transitions from the vibrationally ground state (0,0,0). They are conducted using the same parameters as for the absorption.

Figures 5 and 6 collect the calculated Raman excitation profiles for the ν_1 and ν_3 progressions, respectively, as a function of the excitation photon energy together with the position of the laser wavelength which is used when getting the experimental spectrum. The strongly varying line shapes give a measure of the difficulty in reproducing observed data. This is in particular the case for the I_{002} intensity for which the frequency of the exciting laser is close to a local minimum in the profile and the calculation, very sensitive to the geometry of the potential surface, is unable to give an accurate result. The calculated and observed[10] resonance Raman spectra are plotted in Fig. 7. A few remarks are in order:

(i) A long progression of ν_1 overtones is obtained with a regular decreasing behavior (when I_{200} is taken apart). The differences with observed ratios for far overtones may be due

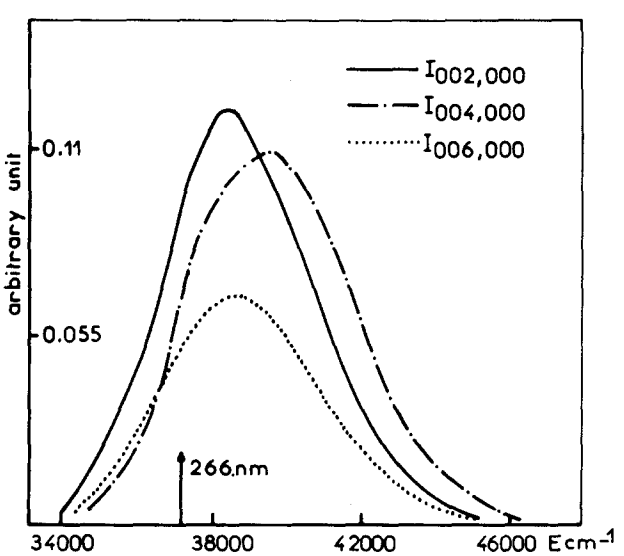

FIG. 6. Raman excitation profiles for the ν_3 progression from the ground (0,0,0) state.

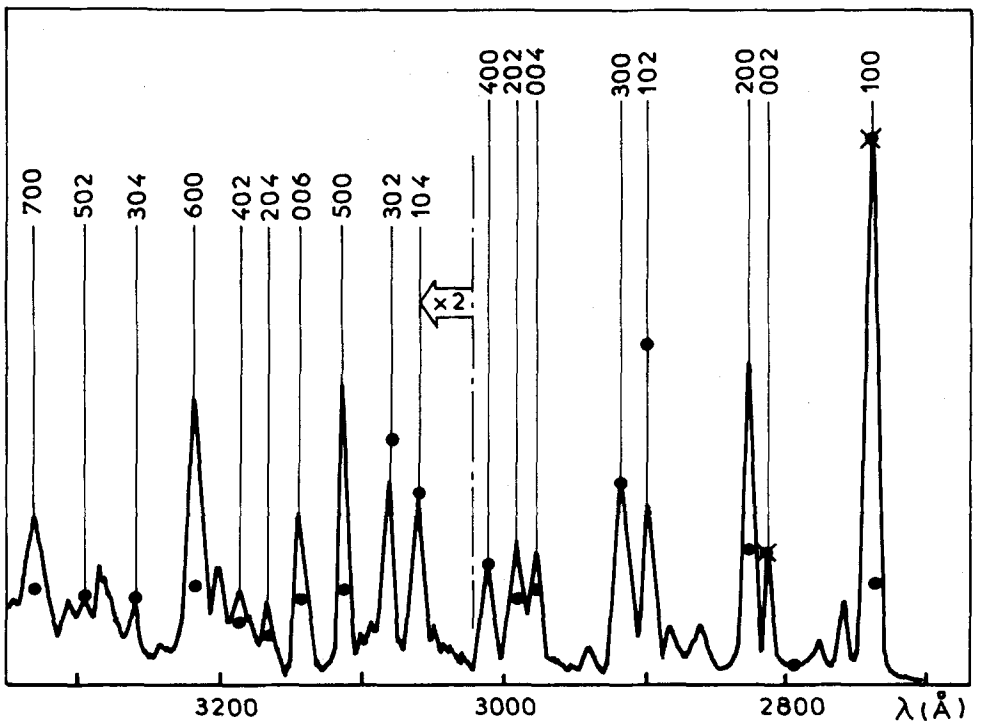

FIG. 7. Photoemission (resonance Raman) spectrum of ozone excited at 266 nm wavelength. The solid line is the experimental data of Ref. 10. The horizontal arrow indicates a scale change (×2). Dots represent the calculated intensities and crosses indicate the calibration values.

to poor estimations of the isolated peak intensities in this region of the spectrum where wide overlappings are present.

(ii) The absence of odd quanta in the q_3 mode is a consequence of the symmetry in our model and has already been commented upon.

(iii) A progression of ν_3 overtones (with even quanta) is calculated and leads to very important intensities. A ratio of ~ 0.6 I_{006}/I_{002} indicates for this mode a behavior very simlar to that of the totally symmetric mode ν_1 with a strong progression as in the observed spectrum.

(iv) The combination bands in ν_1 with either 2 or 4 quanta in ν_3 are of the same order of magnitude than the ν_1 progression and are fairly well given.

(v) When the relative activity of these three modes is compared it turns out that the q_3 mode gives intensities close to that of the q_1 mode with a ratio $I_{002}/I_{100} \sim 1$. As for the intensities of the bands involving the q_2 mode, they are considerably weaker. The first point is not in agreement with experiment and the oversimplified potential barrier seems to be responsible of this discrepancy. The second point follows the experimental observation in which the q_2 mode is not detected. This indicates that the very slight change in bond angle and curvature with respect to the bending is correctly taken into account but the model fails by exaggerating the variations of equilibrium geometry for the antisymmetric stretch between the upper and lower potential surfaces. When different parameters are taken to get a correct fit for this ratio, the absorption line shape is no longer reproduced. Finally, if this difficulty is erased by calibrating the ratios with respect either to I_{00} or to I_{002} one obtains a complete view of the theory–experiment agreement in Fig. 7 where the nonobserved (0,1,0) and (1,1,0) transitions are also indicated. Their intensities are not sufficiently important and their energy positioning in the wing of the (1,0,0) and (0,0,2) bands are such that their assignment is in fact not possible.

ACKNOWLEDGMENTS

The authors wish to thank Professor J. Alberto Beswick for his interest in this work and for helpful discussions. We acknowledge a grant of computing time from the "Conseil Scientifique du Centre de Calcul Vectoriel pour la Recherche."

APPENDIX A

This Appendix is concerned with the calculation of the overlap integral between the continuum wave functions $\chi_\epsilon^\eta(\xi)$:

$$\int_{-\infty}^{\infty} \chi_\epsilon^{\eta*}(\xi)\chi_{\epsilon'}^{\eta}(\xi)d\xi = 2\int_0^{\infty} \chi_\epsilon^{\eta*}(\xi)\chi_{\epsilon'}^{\eta}(\xi)d\xi. \tag{A1}$$

For $\epsilon \neq \epsilon'$, orthogonality of eigenvectors for different eigenvalues imposes a null value, as for $\epsilon = \epsilon'$ the integral is divergent due to the positive values of $|\chi_\epsilon^\eta(\xi)|^2$ at large ξ but can be separated into two parts:

$$\int_0^{\infty} |\chi_\epsilon^\eta(\xi)|^2 d\xi = \int_0^{\xi_0} |\chi_\epsilon^\eta(\xi)|^2 d\xi + \int_{\xi_0}^{\infty} |\chi_\epsilon^\eta(\xi)|^2 d\xi; \tag{A2}$$

the first which is finite and negligible when compared to the second leading to divergency. Furthermore, ξ_0 is chosen in the region of the asymptotic behavior of the wave function, where

$$\chi_\epsilon^\eta(\xi \geqslant \xi_0) = A(\epsilon,\eta)\exp\left(-\frac{i}{2}\xi^2\right)\xi^{-1/2}\xi^{-i\epsilon}. \tag{A3}$$

$A(\epsilon,\eta)$ being defined by Eq. (14) of the main text. Finally the overlap results in

$$\int_{-\infty}^{\infty} \chi_\epsilon^{\eta*}(\xi)\chi_{\epsilon'}^{\eta}(\xi)d\xi = 2|A(\epsilon,\eta)|^2 \int_0^{\infty} \frac{\xi^{i(\epsilon-\epsilon')}}{\xi} d\xi, \tag{A4}$$

where the integral on the right-hand side is nothing but representation for $\pi\delta(\epsilon-\epsilon')$ so that

$$\int_{-\infty}^{\infty}\chi_{\epsilon}^{\eta^*}(\xi)\chi_{\epsilon'}^{\eta}(\xi)d\xi = 4\pi|A(\epsilon,\eta)|^2. \tag{A5}$$

Returning back to the integration variable q_3 and noting that

$$\delta(\epsilon-\epsilon') = \hbar k'^{1/2}_{33}\delta(E_f - E'_f), \tag{A6}$$

the energy-normalization factor appropriate to $\chi^{\eta}_{E_f}(q_3)$ is found to be

$$N^{\eta}(\epsilon) = (2\pi)^{-1}\hbar^{-3/4}k'^{-1/8}_{33}(1-\eta)^{-1} \times\exp(\pi\epsilon/4)|\Gamma(1/4+\eta+i\epsilon/2)|. \tag{A7}$$

APPENDIX B

The two-dimensional overlap integral $W_{v_1v_2}(v'_1,v'_2)$ can be written as

$$W_{v_1v_2}(v'_1,v'_2) = \pi^{-1}(k'_{11}k'_{22}/k_{11}k_{22})^{1/8}(2^{v_1+v_2+v'_1+v'_2}v_1!v_2!v'_1!v'_2!)^{1/2} \times\int_{-\infty}^{\infty}\int_{-\infty}^{\infty}e^{-(r_1^2+r_2^2+r_1'^2+r_2'^2)/2}H_{v_1}(r_1)H_{v_2}(r_2)H_{v'_1}(r'_1)H_{v'_2}(r'_2)J(r,r')dr_1\,dr_2, \tag{B1}$$

where $J(r,r')$ is the Jacobian of the transformation of the normal mass-weighted coordinates given by the linear relation

$$\mathbf{r}' = \tau\mathbf{r}+\delta. \tag{B2}$$

The matrix τ and the column vector δ can easily be found by multiplying **T** and **D** (cf. Table I) with appropriate mass factors. To perform the calculations, we use the variable change described by Faulkner[37] to separate the coordinates in the exponent. Let $s = W^t r$ be the coordinate transformation which diagonalizes $\tau^t\tau$ (t is a notation for the transpose matrix). One has

$$r_1^2+r_2^2 = s_1^2+s_2^2, \tag{B3}$$

$$r_1'^2+r_2'^2 = (G_1^{1/2}s_1+d_1)^2+(G_2^{1/2}s_2+d_2)^2, \tag{B4}$$

where G_1 and G_2 are the eigenvalues of $\tau^t\tau$. The column vector **d** is defined by

$$\mathbf{d} = \mathbf{G}^{1/2}\mathbf{U}^{-1}+\delta \tag{B5}$$

with

$$\mathbf{U} = \tau W. \tag{B6}$$

$W_{v_1v_2}(v'_1,v'_2)$ written in terms of **s** variables results in

$$W_{v_1v_2}(v'_1,v'_2) = \pi^{-1}(k'_{11}k'_{22}/k_{11}k_{22})^{1/8}(2^{v_1+v_2+v'_1+v'_2}v_1!v_2!v'_1!v'_2!)^{1/2} \times\det(\tau)\int_{-\infty}^{\infty}\int_{-\infty}^{\infty}e^{-(s_1^2+s_2^2)/2}e^{-[(G_1^{1/2}s_1+d_1)^2+(G_2^{1/2}s_2+d_2)^2]/2}H_{v_1}(D_1+U_{11}s_1+U_{12}s_2) \times H_{v_2}(D_2+U_{21}s_1+U_{22}s_2)H_{v'_1}(W_{11}s_1+W_{12}s_2)H_{v'_2}(W_{21}s_1+W_{22}s_2)ds_1\,ds_2. \tag{B7}$$

Using the relation[34]

$$2^{n/2}H_n[(x+y)/\sqrt{2}] = \sum_{p=0}^{n}C_n^pH_p(x)H_{n-p}(y) \tag{B8}$$

the double integral of Eq. (B7) can be separated into a sum of products of one-dimensional integrals:

$$W_{v_1v_2}(v'_1,v'_2) = \pi^{-1}(k'_{11}k'_{22}/k_{11}k_{22})^{1/8}\det(\tau)\sum_{a=0}^{v_1}\sum_{b=0}^{v_2}\sum_{c=0}^{v'_1}\sum_{d=0}^{v'_2}C_{v_1}^aC_{v_2}^bC_{v'_1}^cC_{v'_2}^d \times\int_{-\infty}^{\infty}e^{-s_1^2/2}e^{-(G_1^{1/2}s_1+d_1)^2/2}H_a[(D_1+U_{11}s_1)\sqrt{2}]H_b(U_{21}s_1\sqrt{2})H_c(W_{11}s_1\sqrt{2})H_d(W_{21}s_1\sqrt{2})ds_1 \times\int_{-\infty}^{\infty}e^{-s_2^2/2}e^{-(G_2^{1/2}s_2+d_2)/2}H_{v_1-a}(U_{12}s_2\sqrt{2})H_{v_2-b}[(D_2+U_{22}s_2)\sqrt{2}] \times H_{v'_1-c}(W_{12}s_2\sqrt{2})H_{v'_2-d}(W_{22}s_2\sqrt{2})ds_2, \tag{B9}$$

where the C's are binomial coefficients.

At this stage, the calculations may be completed by a numerical evaluation of these one-dimensional integrals. But a complete analytical solution may also be obtained if one expresses the one-dimensional integrals as linear combinations of overlap integrals between two harmonic oscillators with different frequencies and shifted equilibrium positions.

This is done, using the addition formula[46]

$$H_n[xy+(1-x^2)^{1/2}t]=\sum_{p=0}^{n} C_n^p x^{n-p}(1-x^2)^{p/2}H_{n-p}(y)H_p(t) \tag{B10}$$

which results for the integral over s_1 in

$$\begin{aligned}\int_{-\infty}^{\infty} & e^{-s_1^2/2}e^{-(G_1^{1/2}s_1+d_1)^2/2}H_a[(D_1+U_{11}s_1)\sqrt{2}]H_b(U_{21}s_1\sqrt{2})H_c(W_{11}s_1\sqrt{2})H_d(W_{21}s_1\sqrt{2})ds_1 \\ &=\sum_{p=0}^{a}\sum_{q=0}^{b}\sum_{r=0}^{c}\sum_{s=0}^{d} C_a^p C_b^q C_c^r C_d^s (2^{1/2}U_{11}/G_1^{1/2})^{a-p}(2^{1/2}U_{21}/G_1^{1/2})^{b-q} \\ &\times(2^{1/2}W_{11})^{c-r}(2^{1/2}W_{21})^{d-s}(1-2U_{11}^2/G_1)^{p/2}(1-2U_{21}^2/G_1)^{q/2}(1-2W_{11}^2)^{r/2}(1-2W_{21}^2)^{s/2} \\ &\times H_p[(2^{1/2}D_1G_1^{1/2}-2^{1/2}U_{11}d_1)/(G_1-2U_{11}^2)^{1/2}]H_q[-2^{1/2}U_{21}d_1/(G_1-2U_{21})^{1/2}]H_r(0)H_s(0) \\ &\times\int_{-\infty}^{\infty} e^{-s_1^2/2}e^{-(G_1^{1/2}s_1+d_1)^2/2}H_{a-p}(G_1^{1/2}s_1+d_1)H_{b-q}(G_1^{1/2}s_1+d_1)H_{c-r}(s_1)H_{d-s}(s_1)ds_1.\end{aligned} \tag{B11}$$

A similar expression holds for the integral over s_2.

A last transformation is the linear expansion of the product of two Hermite polynomials[46]:

$$H_m(x)H_n(x)=\sum_{r=0}^{\inf(n,m)} 2^r r! C_m^r C_n^r H_{m+n-2r}(x) \tag{B12}$$

which gives

$$\begin{aligned}\int_{-\infty}^{\infty} & e^{-s_1^2/2}e^{-(G_1^{1/2}s_1+d_1)^2/2}H_{a-p}(G_1^{1/2}s_1+d_1)H_{b-q}(G_1^{1/2}s_1+d_1)H_{c-r}(s_1)H_{d-s}(s_1)ds_1 \\ &=\sum_{u=0}^{\inf(a-p,b-q)}\sum_{v=0}^{\inf(c-r,d-s)} 2^{u+v}u!v!C_{a-p}^u C_{b-q}^u C_{c-r}^v C_{d-s}^v \\ &\times\int_{-\infty}^{\infty} e^{-s_1^2/2}e^{-(G_1^{1/2}s_1+d_1)^2/2}H_{a+b-p-q-2u}(G_1^{1/2}s_1+d_1)H_{c+d-r-s-2v}(s_1)ds_1.\end{aligned} \tag{B13}$$

The integrals on the right-hand side of Eq. (B13) are those describing the overlap between two displaced harmonic oscillators with different frequencies and are evaluated using the recursive formula given by Manneback.[38]

APPENDIX C

This Appendix is devoted to the calculation of the transition probability of Raman scattering $\mathscr{A}_{\tilde{v}_3 v_3}$ given by[39]

$$\mathscr{A}_{\tilde{v}_3 v_3}(\bar{\epsilon})=\lim_{\alpha\to 0^+}\int \frac{\langle\chi_{\tilde{v}_3}|\chi_\epsilon^\eta\rangle\langle\chi_\epsilon^\eta|\chi_{v_3}\rangle}{\bar{\epsilon}-\epsilon+i\alpha}d\epsilon, \tag{C1}$$

where $\bar{\epsilon}$ is related to the energy brought by the incoming photon into the dissociative mode q_3.

Within the parabolic barrier model, this integral may be analytically evaluated. A general way for this derivation introduces the relation

$$\frac{1}{\bar{\epsilon}-\epsilon+i\alpha}=-i\int_0^\infty e^{i(\bar{\epsilon}-\epsilon+i\alpha)\tau}d\tau \tag{C2}$$

into Eq. (C1) which leads to a double integral:

$$\mathscr{A}_{\tilde{v}_3 v_3}(\bar{\epsilon})=-i\int_0^\infty\left(\int_{-\infty}^{\infty} e^{i(\bar{\epsilon}-\epsilon+i\alpha)\tau}\langle\chi_{\tilde{v}_3}|\chi_\epsilon^\eta\rangle\langle\chi_\epsilon^\eta|\chi_{v_3}\rangle d\epsilon\right)d\tau. \tag{C3}$$

Equation (31) together with the expansion of the hypergeometric function ${}_2F_1(a,b;c,z)$ in terms of finite series allow us to write the product of the two overlap integrals as

$$\begin{aligned}\langle\chi_{\tilde{v}_3}|\chi_\epsilon^\eta\rangle\langle\chi_\epsilon^\eta|\chi_{v_3}\rangle &= (\hbar^2 k'_{33})^{-1/2}\chi^{\eta-1/4}2^{6\eta-p-\tilde{p}-1}\frac{(\tilde{v}_3!)^{1/2}(v_3!)^{1/2}}{p!\tilde{p}!}\frac{[\Gamma(\frac{1}{2}+2\eta)]^4}{\pi^{5/2}(1-\eta)^2}e^{\epsilon\gamma}(-1)^{p+\tilde{p}} \\ &\times\sum_{q=0}^{p}\sum_{\tilde{q}=0}^{\tilde{p}}(-1)^{q+\tilde{q}}2^{q+\tilde{q}}C_p^q C_{\tilde{p}}^{\tilde{q}}(1+\chi)^{-(4\eta+q+\tilde{q}+1)/2}\frac{e^{-1/2(q-\tilde{q})(\gamma-\pi/2)}}{\Gamma(2\eta+1/2+q)\Gamma(2\eta+1/2+\tilde{q})} \\ &\times\sum_{s=0}^{q}\sum_{\tilde{s}=0}^{\tilde{q}}\Gamma\begin{bmatrix}\frac{1}{4}+q+\eta+i(\epsilon/2),\frac{3}{4}-q-\eta-i(\epsilon/2),\frac{1}{4}+\eta+s-i(\epsilon/2)\\ \frac{1}{4}+\eta-i(\epsilon/2),\frac{3}{4}-q-\eta+s+i(\epsilon/2)\end{bmatrix} \\ &\times\Gamma\begin{bmatrix}\frac{1}{4}+\tilde{q}+\eta-i(\epsilon/2),\frac{3}{4}-\tilde{q}-\eta+i(\epsilon/2),\frac{1}{4}+\eta+\tilde{s}+i(\epsilon/2)\\ \frac{1}{4}+\eta+i(\epsilon/2),\frac{3}{4}-\tilde{q}-\eta-\tilde{s}+i(\epsilon/2)\end{bmatrix} \\ &\times\frac{\Gamma(-q+s)\Gamma(-\tilde{q}+\tilde{s})}{\Gamma(-q)\Gamma(-\tilde{q})}\frac{1}{s!\tilde{s}!}\left(\frac{1-i\chi^{1/2}}{1+i\chi^{1/2}}\right)^{s-\tilde{s}}\end{aligned} \tag{C4}$$

with the notation

$$\Gamma\begin{bmatrix} a_1,a_2,\ldots,a_n \\ b_1,b_2,\ldots,b_m \end{bmatrix} = \frac{\Gamma(a_1)\Gamma(a_2)\cdots\Gamma(a_n)}{\Gamma(b_1)\Gamma(b_2)\cdots\Gamma(b_m)}. \tag{C5}$$

The first integration is to be carried over ϵ. An appropriate change of variable $\theta = i\epsilon/2$ gives

$$\begin{aligned}\int_{-\infty}^{\infty} \langle \chi_{\tilde{v}_3}|\chi_\epsilon^\eta\rangle\langle\chi_\epsilon^\eta|\chi_{v_3}\rangle e^{-i\epsilon\tau}\,d\epsilon = (\hbar^2 k'_{33})^{-1/2}\chi^{\eta-1/4}2^{6\eta-p-\tilde{p}-1}\frac{(\tilde{v}_3!)^{1/2}(v_3!)^{1/2}}{p!\tilde{p}!}\frac{[\Gamma(\frac{1}{2}+2\eta)]^4}{\pi^{5/2}(1-\eta)^2}(-1)^{p+\tilde{p}} \\ \times\sum_{q=0}^{p}\sum_{\tilde{q}=0}^{\tilde{p}}(-1)^{q+\tilde{q}}2^{q+\tilde{q}}C_p^q C_{\tilde{p}}^{\tilde{q}}(1+\chi)^{-(4\eta+q+\tilde{q}+1)/2}\frac{e^{-i/2(q-\tilde{q})(\gamma-\pi/2)}}{\Gamma(2\eta+\frac{1}{2}+q)\Gamma(2\eta+\frac{1}{2}+\tilde{q})} \\ \times\sum_{s=0}^{q}\sum_{\tilde{s}=0}^{\tilde{q}} Y\frac{\Gamma(-q+s)\Gamma(-\tilde{q}+\tilde{s})}{\Gamma(-q)\Gamma(-\tilde{q})}\frac{1}{s!\tilde{s}!}\left(\frac{1-i\chi^{1/2}}{1+i\chi^{1/2}}\right)^{s-\tilde{s}}\end{aligned} \tag{C6}$$

with

$$\begin{aligned}Y = -2i\int_{-i\infty}^{i\infty}\Gamma\begin{bmatrix}\frac{1}{4}+q+\eta+\theta,\frac{3}{4}-q-\eta-\theta,\frac{1}{4}+\eta+s+\theta \\ \frac{1}{4}+\eta-\theta,\frac{3}{4}-q-\eta+s-\theta\end{bmatrix} \\ \times\Gamma\begin{bmatrix}\frac{1}{4}+\tilde{q}+\eta-\theta,\frac{3}{4}-\tilde{q}-\eta+\theta,\frac{1}{4}+\eta+s+\theta \\ \frac{1}{4}+\eta+\theta,\frac{3}{4}-\tilde{q}-\eta+\tilde{s}+\theta\end{bmatrix} e^{-2i(\gamma-i\tau)}\,d\theta.\end{aligned} \tag{C7}$$

Slater (cf. Ref. 45, p. 22) showed that the relation

$$\frac{\Gamma(1-z)}{\Gamma(1-z+n)} = (-1)^n\frac{\Gamma(z-n)}{\Gamma(z)} \tag{C8}$$

together with a contour integration lead to the evaluation of Y [Eq. (C7)]. The poles which contribute to the integral are the solutions of $1/4+\tilde{q}+\eta-\theta = -n$, n being a positive integer. The result is expressed as an infinite series over these poles:

$$Y = 4\pi\sum_{n=0}^{\infty}\Gamma\begin{bmatrix}\frac{1}{2}+q+\tilde{q}+2\eta-s+n,1+\tilde{q}+n,1+n,\frac{1}{2}+2\eta+\tilde{q}+\tilde{s}+n \\ 1+\tilde{q}-s+n,\frac{1}{2}+\tilde{q}+2\eta+n,1+\tilde{s}+n\end{bmatrix}\frac{(1)^n}{n!}e^{-2i(\gamma-i\tau)(n+\tilde{q}+\eta+1/4)} \tag{C9}$$

which can in turn be expressed as a hypergeometric function ${}_4F_3$:

$$\begin{aligned}Y = 4\pi e^{-2i(\gamma-i\tau)(\tilde{q}+\eta+1/4)}\Gamma\begin{bmatrix}\frac{1}{2}+q+\tilde{q}-s+2\eta,1+\tilde{q},1,\frac{1}{2}+2\eta+\tilde{q}+\tilde{s} \\ 1+\tilde{q}-s,\frac{1}{2}+\tilde{q}+2\eta,1+\tilde{s}\end{bmatrix} \\ \times{}_4F_3\begin{bmatrix}\frac{1}{2}+q+\tilde{q}-s+2\eta,1+\tilde{q},1,\frac{1}{2}+2\eta+\tilde{q}+\tilde{s}; -e^{-2i(\gamma-i\tau)} \\ 1+\tilde{q}-\tilde{s},\frac{1}{2}+\tilde{q}+2\eta,1+\tilde{s};\end{bmatrix}.\end{aligned} \tag{C10}$$

The last integration over τ in Eq. (C3) leads to integrals of the form

$$Z = \int_0^{\infty} e^{i\bar{\epsilon}\tau}e^{-2\tau(\tilde{q}+\eta+\frac{1}{4})}{}_4F_3\begin{bmatrix}a_1,a_2,a_3,a_4; -e^{-2i(\gamma-i\tau)} \\ b_1,b_2,b_3;\end{bmatrix}d\tau \tag{C11}$$

which have also been studied by Slater (Ref. 45, p. 108). Their evaluation proceeds through the change of variable $t = e^{-2\tau}$. One obtains

$$Z = \tfrac{1}{2}\Gamma\begin{bmatrix}\frac{1}{4}+\tilde{q}+\eta-i(\bar{\epsilon}/2) \\ \frac{5}{4}+\tilde{q}+\eta-i(\bar{\epsilon}/2)\end{bmatrix}{}_5F_4\begin{bmatrix}\frac{1}{4}+\tilde{q}+\eta-i(\bar{\epsilon}/2),a_1,a_2,a_3,a_4;e^{-2i\gamma} \\ \frac{5}{4}+\tilde{q}+\eta-i(\bar{\epsilon}/2),b_1,b_2,b_3;\end{bmatrix} \tag{C12}$$

and one can deduce the general expression for the Raman amplitude

$$\begin{aligned}\mathscr{A}_{\tilde{v}_3v_3}(\bar{\epsilon}) = -i(\hbar^2k'_{33})^{-1/2}\chi^{\eta-1/4}2^{6\eta-p-\tilde{p}}\frac{(\tilde{v}_3!)^{1/2}(v_3!)^{1/2}}{\tilde{p}!p!}(-1)^{p+\tilde{p}}\frac{[\Gamma(1/2+2\eta)]^4}{\pi^{3/2}(1-\eta)^2} \\ \times\sum_{q=0}^{p}\sum_{\tilde{q}=0}^{\tilde{p}}(-1)^{q+\tilde{q}}2^{q+\tilde{q}}C_p^qC_{\tilde{p}}^{\tilde{q}}(1+\chi)^{-(4\eta+q+\tilde{q}+1)/2}\frac{e^{-1/2(q-\tilde{q})(\gamma-\pi/2)}}{\Gamma(2\eta+1/2+q)\Gamma(2\eta+1/2+\tilde{q})} \\ \times\sum_{s=0}^{q}\sum_{\tilde{s}=0}^{q}\left(e^{-2i\gamma(1/4+\tilde{q}+\eta)}\Gamma\begin{bmatrix}\frac{1}{4}+\tilde{q}+\eta-i(\bar{\epsilon}/2),\frac{1}{2}+q+\tilde{q}-s+2\eta,1+\tilde{q},1,1/2+2\eta+\tilde{q}+\tilde{s} \\ \frac{5}{4}+\tilde{q}+\eta-i(\bar{\epsilon}/2),1+\tilde{q}-\tilde{s},\frac{1}{2}+\tilde{q}+2\eta,1+\tilde{s}\end{bmatrix}\right. \\ \times{}_5F_4\begin{bmatrix}\frac{1}{2}+\eta-i(\bar{\epsilon}/2),\frac{1}{2}+q+\tilde{q}-s+2\eta,1+\tilde{q},1,\frac{1}{2}+2\eta+\tilde{q}+\tilde{s}; -e^{-2i\gamma} \\ \frac{5}{4}+\tilde{q}+\eta-i(\bar{\epsilon}/2),1+\tilde{q}-s,\frac{1}{2}+\tilde{q}+2\eta,1+s;\end{bmatrix} \\ \left.\times\frac{\Gamma(-q+s)\Gamma(-\tilde{q}+\tilde{s})}{\Gamma(-q)\Gamma(-\tilde{q})}\frac{1}{s!\tilde{s}!}\left(\frac{1-i\chi}{1+i\chi}\right)^{s-\tilde{s}}\right).\end{aligned} \tag{C13}$$

For the transitions $\mathscr{A}_{\tilde{v}_30}$ which are the most important, this expression simplifies to

$$\mathscr{A}_{\tilde{v}_3 0}(\bar{\epsilon}) = -(\hbar^2 k'_{33})^{-1/2}\chi^{-1/4}(1+\chi)^{-1/4}\frac{(\tilde{v}_3!)^{1/2}}{\tilde{p}!}\frac{(-1)^{\tilde{p}}}{2^{\tilde{p}}}\sum_{\tilde{q}=0}^{\tilde{p}}(-1)^{\tilde{q}}2^{\tilde{q}}\frac{C_{\tilde{p}}^{\tilde{q}}}{\Gamma(\tilde{q}+\frac{1}{2})}(1+\chi)^{-(\tilde{q}+1/2)/2}$$
$$\times e^{-i(\tilde{q}/2)(\gamma-\pi/2)}\sum_{\tilde{s}=0}^{\tilde{q}}\frac{\Gamma(-\tilde{q}+\tilde{s})\Gamma(1/2+\tilde{q}+\tilde{s})}{\Gamma(-\tilde{q})\Gamma(1+\tilde{s})}\frac{\Gamma[1/4+\tilde{q}-i(\bar{\epsilon}/2)]}{\Gamma[5/4+\tilde{q}-i(\bar{\epsilon}/2)]}e^{-i\gamma(1/2+\tilde{q})}$$
$$\times {}_3F_2[-i(\bar{\epsilon}/2)+\tilde{q}+1/4,1,1/2+\tilde{q}+\tilde{s};-i(\bar{\epsilon}/2)+\tilde{q}+5/4,1+\tilde{s};-e^{-2i\gamma}]\frac{1}{\tilde{s}!}\left(\frac{1-i\chi^{1/2}}{1+i\chi^{1/2}}\right)^{\tilde{s}}. \quad \text{(C14)}$$

Using the relation

$${}_2F_1[1/4-i(\bar{\epsilon}/2),1/2;5/4-i(\bar{\epsilon}/2);-e^{-2i\gamma}]$$
$$=\frac{\Gamma[5/4-i(\bar{\epsilon}/2)]\Gamma[1/4+i(\bar{\epsilon}/2)]}{\pi^{1/2}}e^{i\gamma/2}e^{\gamma\bar{\epsilon}}{}_2F_1[1/4-i(\bar{\epsilon}/2),0;3/4-i(\bar{\epsilon}/2);-e^{-2i\gamma}]$$
$$+\frac{\Gamma[5/4-i(\bar{\epsilon}/2)]\Gamma[-1/4-i(\bar{\epsilon}/2)]}{\Gamma[1/4-i(\bar{\epsilon}/2)]\Gamma[3/4-i(\bar{\epsilon}/2)]}e^{i\gamma}{}_2F_1[1/2,1/4-i(\bar{\epsilon}/2),5/4+i(\bar{\epsilon}/2);-e^{-2i\gamma}] \quad \text{(C15)}$$

the optical theorem can be verified:

$$-\frac{1}{\pi}\mathrm{Im}(\mathscr{A}_{00}) = (\hbar^2 k'_{33})^{-1/2}\chi^{-1/4}(1+\chi)^{-1/2}\frac{|\Gamma[1/4+i(\bar{\epsilon}/2)]|^2}{2\pi^{3/2}}e^{\gamma\bar{\epsilon}} \quad \text{(C16)}$$

by noticing that the right-hand side of Eq. (C16) is nothing but the Franck–Condon factor corresponding to the incoming photon at energy $\bar{\epsilon}$.

[1] J. E. Davenport, *Parameters of Ozone Photolysis as a Function of Temperature at 280–330 nm* (Office of Environment and Energy, Washington, D.C., 1980).
[2] A. M. Bass and R. J. Paur, J. Photochem. **17**, 141 (1981).
[3] M. Griggs, J. Chem. Phys. **49**, 857 (1978).
[4] A. G. Heam, Proc. Phys. Soc. London **78**, 932 (1961).
[5] J. W. Simons, R. J. Paur, H. A. Webster, and E. J. Bair, J. Chem. Phys. **59**, 1203 (1973).
[6] E. Vigroux, Ann. Phys. (Paris) **8**, 709 (1953); C. R. Acad. Sci. (Paris) **234**, 2439, 2592 (1952).
[7] D. C. Astholz, A. E. Croce, and J. Troe, J. Chem. Phys. **86**, 696 (1982).
[8] W. M. Jones and N. Davidson, J. Am. Chem. Soc. **84**, 2868 (1962).
[9] J. A. Hanvey and W. D. McGrath, Chem. Phys. Lett. **36**, 564 (1975).
[10] D. G. Imre, J. L. Kinsey, R. M. Field, and D. H. Katayama, J. Phys. Chem. **86**, 2564 (1982).
[11] P. J. Hay and T. H. Dunning, Jr., J. Chem. Phys. **76**, 2290 (1977).
[12] G. D. Carney, L. A. Curtiss, and S. R. Langhoff, J. Mol. Spectrosc. **61**, 371 (1976).
[13] P. J. Hay, R. T Pack, R. B. Walker, and E. J. Heller, J. Phys. Chem. **86**, 862 (1982).
[14] J. N. Murrel, K. S. Sorbie, and A. J. C. Varandas, Mol. Phys. **32**, 1359 (1976).
[15] J. N. Murrel and S. Farantos, Mol. Phys. **34**, 1185 (1977).
[16] E. J. Heller, J. Chem. Phys. **75**, 2923 (1981).
[17] S. M. Adler-Golden, J. Quant. Spectrosc. Radiat. Transfer **30**, 175 (1983).
[18] O. Atabek, S. Miret-Artes, and M. Jacon, J. Chem. Phys. **83**, 1769 (1985).
[19] G. C. Shatz and A. Kuppermann, J. Chem. Phys. **65**, 4642 (1976).
[20] M. Shapiro and G. G. Balint-Kurti, J. Chem. Phys. **71**, 1461 (1979).
[21] E. Segev and M. Shapiro, J. Chem. Phys. **77**, 5604 (1982).
[22] O. Atabek and R. Lefebvre, Phys. Rev. A **22**, 1817 (1980); Chem. Phys. **52**, 199 (1980).
[23] R. T Pack, J. Chem. Phys. **65**, 4765 (1976).
[24] J. O. Hirschfelder, C. F. Curtiss, and R. B. Bird, *Molecular Theory of Gases and Liquids* (Wiley, New York, 1954).
[25] R. A. Marcus, J. Chem. Phys. **45**, 4493 (1966).
[26] J. C. Light, Adv. Chem. Phys. **19**, 1 (1971).
[27] M. G. Sheppard and R. B. Walker, J. Chem. Phys. **78**, 7191 (1983).
[28] A. Barbe, C. Secroun, and P. Jouve, J. Mol. Spectrosc. **49**, 171 (1974).
[29] M. Shapiro and R. Bersohn, Annu. Rev. Phys. Chem. **33**, 409 (1982).
[30] Plotnikov, Opt. Spectrosc. **29**, 453 (1970).
[31] J. N. L. Connor, Mol. Phys. **15**, 37 (1968).
[32] M. Abramowitz and I. Stegun, *Handbook of Mathematical Functions* (Dover, New York, 1968).
[33] I. S. Gradshteyn and I. M. Ryzhik, *Table of Integrals, Series, and Products* (Academic, New York, 1965).
[34] W. Magnus, F. Oberhettinger, and R. P. Soni, *Formulas and Theorems for the Special Functions of Mathematical Physics* (Springer, Berlin, 1966).
[35] M. D. Morse and K. F. Freed, J. Chem. Phys. **78**, 6045 (1983).
[36] O. Atabek and R. Lefebvre, Chem. Phys. **23**, 51 (1977).
[37] T. R. Faulkner and F. S. Richardson, J. Chem. Phys. **70**, 1201 (1979).
[38] C. Manneback, Physica **17**, 1001 (1951).
[39] O. Atabek, R. Lefebvre, and M. Jacon, J. Chem. Phys. **72**, 2670 (1980).
[40] K. Kodama and Y. Mori, Chem. Phys. **46**, 371 (1980).
[41] E. C. Y. Inn and Y. Tanaka, J. Opt. Soc. Am. **43**, 870 (1953).
[42] J. Brion, D. Daumont, J. Malicet, and P. Marche (private communication).
[43] M. Mingardi, W. Siebrand, D. Van Labeke, and M. Jacon, Chem. Phys. Lett. **31**, 208 (1975).
[44] E. J. Heller, R. Sundberg, and D. Tannor, J. Phys. Chem. **86**, 1882 (1982).
[45] L. J. Slater, *Generalized Hypergeometric Functions* (Cambridge University, Cambridge, 1966).
[46] N. Ja. Vilenkin, *Fonctions Speciales et Theorie de la Representation des Groupes* (Dunod, Paris, 1969).